Published in final edited form as:
J Immunol. 2010 January 15; 184(2): 1031–1040. doi:10.4049/jimmunol.0902773.

CD8 T Cell-Initiated Vascular Endothelial Growth Factor Expression Promotes Central Nervous System Vascular Permeability under Neuroinflammatory Conditions

Georgette L. Suidan[*,†], **Jonathan W. Dickerson**[*,†], **Yi Chen**[†], **Jeremiah R. McDole**[*,†], **Pulak Tripathi**[‡], **Istvan Pirko**[*,†], **Kim B. Seroogy**[*,†], and **Aaron J. Johnson**[*,†]

[*] Neuroscience Graduate Program, University of Cincinnati College of Medicine, Cincinnati, OH 45267

[†] Department of Neurology, University of Cincinnati College of Medicine, Cincinnati, OH 45267

[‡] Division of Immunobiology, Cincinnati Children's Hospital, Cincinnati, OH 45267

Abstract

Dysregulation of the blood-brain barrier (BBB) is a hallmark feature of numerous neurologic disorders as diverse as multiple sclerosis, stroke, epilepsy, viral hemorrhagic fevers, cerebral malaria, and acute hemorrhagic leukoencephalitis. CD8 T cells are one immune cell type that have been implicated in promoting vascular permeability in these conditions. Our laboratory has created a murine model of CD8 T cell-mediated CNS vascular permeability using a variation of the Theiler's murine encephalomyelitis virus system traditionally used to study multiple sclerosis. Previously, we demonstrated that CD8 T cells have the capacity to initiate astrocyte activation, cerebral endothelial cell tight junction protein alterations and CNS vascular permeability through a perforin-dependent process. To address the downstream mechanism by which CD8 T cells promote BBB dysregulation, in this study, we assess the role of vascular endothelial growth factor (VEGF) expression in this model. We demonstrate that neuronal expression of VEGF is significantly upregulated prior to, and coinciding with, CNS vascular permeability. Phosphorylation of fetal liver kinase-1 is significantly increased early in this process indicating activation of this receptor. Specific inhibition of neuropilin-1 significantly reduced CNS vascular permeability and fetal liver kinase-1 activation, and preserved levels of the cerebral endothelial cell tight junction protein occludin. Our data demonstrate that CD8 T cells initiate neuronal expression of VEGF in the CNS under neuroinflammatory conditions, and that VEGF may be a viable therapeutic target in neurologic disease characterized by inflammation-induced BBB disruption.

Disruption of the blood-brain barrier (BBB) is a hallmark feature of numerous neurologic disorders as diverse as multiple sclerosis (MS), stroke, epilepsy, viral hemorrhagic fevers, cerebral malaria, and acute hemorrhagic leukoencephalitis (1–9). Among these diseases, studies in viral hemorrhagic fevers and cerebral malaria have implied a role for CD8 T cells in promoting vascular permeability (10,11).

Dengue fever has been the most widely studied viral hemorrhagic condition, affecting up to 100 million people worldwide (12). Prior exposure to dengue virus primes individuals to

Address correspondence and reprint requests to Dr. Aaron J. Johnson, The Waddell Center for Multiple Sclerosis, 231 Albert Sabin Way, Medical Sciences Building, Room 7011, Academic Health Center, Cincinnati, OH 45267. johna4@uc.edu.

Disclosures
The authors have no financial conflicts of interest.

become susceptible to the hemorrhagic condition on subsequent exposure with a second dengue virus strain (10,13,14). The hemorrhagic phase of dengue is characterized by activation, expansion, and apoptosis of dengue Ag-specific CD8 T cells in the blood of patients (10). Epidemiological studies have further determined that specific HLA class I alleles predispose individuals to dengue hemorrhagic fever (DHF) (15). Alterations in vasculature are also observed in human cerebral malaria, in which an important role for perforin and CD8 T cells has been proposed to contribute to pathogenesis (11,16–18). Therefore, defining the mechanisms by which CD8 T cells and other immune cell types promote BBB disruption is of paramount importance for understanding neurologic diseases, as well as development of therapeutic strategies to treat or prevent these conditions.

To study the interaction between Ag-specific CD8 T cells and the neurovascular unit under inflammatory conditions, our laboratory has developed an in vivo model of CNS vascular permeability using a variation of the Theiler's murine encephalomyelitis virus (TMEV) model of MS. We have termed this model of CD8 T cell initiated BBB disruption peptide-induced fatal syndrome (PIFS) (19–22). PIFS is induced through i.v. administration of Ag that CD8 T cells have TCR specificity for. During acute TMEV infection, 50–70% of CNS-infiltrating CD8 T cells are specific for the Ag viral peptide (VP), $VP2_{121–130}$, presented in context of the D^b class I molecules in the C57BL/6 mouse (23,24). I.v. injection of $VP2_{121–130}$ peptide during the peak of this CD8 T cell expansion in the brain results in a fatal condition characterized by astrocyte activation, cerebral endothelial cell (CEC) tight junction alterations and severe vascular permeability all of which are contingent on perforin expression (22). The rapid induction of BBB disruption through i.v. injection of peptide enables an analysis of downstream events in the CNS that ensue after activation of a specific subset of T cells (13).

Using the PIFS model system, we investigated the importance of vascular endothelial growth factor (VEGF) cytokine in T cell-induced BBB disruption. VEGF was originally termed "vascular permeability factor" by Senger et al. because of its highly vascular-permeating effect that is 50,000-fold more potent than histamine (25–28). After insult to the CNS, altered expression of VEGF and its receptors, FMS-related tyrosine kinase-1 and fetal liver kinase-1 (flk-1), has been observed in various pathological conditions such as ischemia, MS, viral infection, and injury (29–35). On binding VEGF, flk-1 dimerizes and undergoes phosphorylation at several tyrosine residues. The ensuing signal transduction though flk-1 promotes angiogenesis and vascular permeability, strongly implicating a role for VEGF in BBB disruption (28). A complete mechanism by which VEGF contributes to BBB dysregulation under neuroinflammatory conditions has yet to be elucidated (36–38). However, because of its vascular permeating effects in previous studies, we hypothesized that VEGF expression in the CNS contributes to CEC tight junction changes and BBB disruption during neuroinflammatory conditions. Using the PIFS model of CNS vascular permeability, we addressed the timing and downstream mechanisms by which VEGF promotes vascular permeability in the brain. The studies put forward in this paper demonstrate that VEGF contributes to CNS vascular permeability in the PIFS model. We further link VEGF binding to the flk-1 receptor to downregulation of the tight junction protein occludin. Our findings further imply that VEGF inhibition may have therapeutic implications for neurologic diseases characterized by neuroinflammation and BBB alterations.

Methods and Materials

Animals

C57BL/6 (strain no. 000664) and C57BL/6 $Prf1^{-/-}$ ($Prf1^{-/-}$, perforin-deficient; strain no. 002407) mice were obtained from The Jackson Laboratory (Bar Harbor, ME) at 6 wk of age. Animals were given food and water ad libitum. All experiments were approved by the

Institutional Animal Care and Use Committee of the University of Cincinnati (Protocol 06-10-09-01).

Induction of CNS vascular permeability using the PIFS model

CNS vascular permeability was induced as described previously (19,22). Briefly, C57BL/6 mice were infected i.c. with 2×10^6 PFU Daniel's strain of TMEV. Seven days post-TMEV infection, mice were injected i.v. with 0.1 mg $VP2_{121–130}$ (FHAGSLLVFM) (GenScript, Piscataway, NJ) (19) and euthanized 0, 2, 4, 12, and 24 h ($n = 4$ mice for each time point) post-administration of $VP2_{121–130.}$ Brains were excised, frozen on dry ice, and subsequently processed for FITC-albumin leakage, immunofluorescent staining, in situ hybridization, and Western blot. For C57BL/6 $Prf1^{-/-}$ studies, groups of four mice were infected i.c. with 2×10^6 PFU Daniel's strain of TMEV. Seven days post-TMEV infection, mice were injected i.v. with 0.1 mg $VP2_{121–130}$ or E7 control peptide (RAHYNIVTF) and euthanized 24 h later. Brains were excised, frozen on dry ice, and stored at −80°C.

Neuropilin-1 inhibition with ATWLPPR peptide

C57BL/6 mice were infected i.c. with 2×10^6 PFU Daniel's strain of TMEV. Seven days post-TMEV infection, mice were injected i.v. with 0.1 mg $VP2_{121–130}$ or 0.1 mg E7 control peptide (19). ATWLPPR peptide at 1 mg or 3 mg, PBS (vehicle control) or 3 mg of RAPTLWP (scrambled peptide control) (GenScript), was i.v. injected via the tail vein 30 min prior to $VP2_{121–130}$ administration, and 3, 6, and 9 h postadministration of $VP2_{121–130}$ ($n = 6$ mice per group). One hour prior to brain harvest, mice were administered FITC-albumin i.v. Mice were euthanized 12 h post-administration of $VP2_{121–130}$ or E7 control peptide Brains were harvested, the hemisphere ipsilateral to TMEV infection was processed for FITC-albumin leakage, and the contralateral hemisphere was processed for Western blot analysis of occludin protein levels.

FITC-albumin permeability assay

Mice were injected i.v. via the tail vein with 10 mg FITC-albumin (Sigma-Aldrich, St. Louis, MO) 1 h prior to harvest. Fresh-frozen brains were sectioned (10-μm thickness) in a −20°C Microm cryostat (Microm International GmbH, Walldorf, Germany) and thaw-mounted onto VWR micro slides (VWR International, West Chester, PA). Mounted sections were stored at −20°C. All sections not mounted on slides were used to make homogenates as described in the Western blot section (22). Homogenates were normalized for protein using the bicinchoninic acid protein assay (Pierce, Rockford, IL) and read on a fluorescent plate reader at 488 nm excitation and 525 nm emission to detect FITC-albumin leakage into the brain. Data were collected using SpectraMax software (Molecular Devices, Sunnyvale, CA).

Western blots for VEGF and phosphorylated flk-1

Brain tissue samples were lysed in radioimmunoprecipitation assay buffer (10 mmol/l Tris, 140 mmol/l NaCl, 1% Triton X-100, 1% Na deoxycholate, 0.1% SDS, and protease inhibitor mixture [Pierce] pH 7.5) and centrifugated for 30 min at 10,000 rpm. Samples were normalized using the bicinchoninic acid protein assay and prepared using the method of Laemmli (39). Thirty micrograms of sample were loaded per well on 4–20% Tris-HCl gels (Bio-Rad, Hercules, CA) and run using Tris-HCl running buffer. Gels were transferred onto Immun-Blot polyvinylidene difluoride membranes (Bio-Rad, Hercules, CA) using Tris transfer buffer. Blots were blocked for 1 h in 10% PBS-T milk and overnight at 4°C in PhosphoDetect rabbit anti-VEGFR2 ($pTyr^{1054/1059}$) (1:1000) (Calbiochem, San Diego, CA) or rabbit anti-VEGF (1:200) (Calbiochem). Goat anti-rabbit conjugated to HRP (Santa Cruz Biotechnology, Santa Cruz, CA) was used to detect primary Ab. Western blot films were analyzed using OD measurements (Scion Image software [National Institutes of Health]). Background was subtracted from each band and data are expressed in arbitrary units (AU).

Microvessel isolation and tight junction Western blots

Microvessel isolation was based on the protocol previously described by Brooks et al. (40). Briefly, brain hemispheres contralateral to the intracranial TMEV injection site were homogenized in microvessel isolation buffer, 26% dextran was added and samples were centrifuged for 10 min at 5600×*g* (SS-34 rotor, Sorvall, Ramsey, MN). Supernatants were discarded and the pellet was resuspended in microvessel isolation buffer. Samples were centrifuged at 5000×*g* for 10 min. Pellets were resuspended in 6 M urea and digested overnight at 4°C. Protein concentration was determined using a BSA standard curve and 34 μg was added per well to 4–20% Tris-HCl gels (Bio-Rad). For tight junction analysis, blots were probed using mouse anti-GAPDH (1:5000) (Fitzgerald Industries International, Concord, MA) or rabbit anti-occludin (1:500) (Zymed Laboratories, San Francisco, CA). Goat anti-rabbit conjugated to HRP (Santa Cruz Biotechnology) or goat anti-mouse conjugated to horseradish-peroxidase (Santa Cruz Biotechnology) was used to detect primary Ab. Blots were developed and analyzed as described previously in the Western blot section. Occludin samples were normalized for protein with GAPDH values.

In situ hybridization

Fresh-frozen brains were mounted onto TBS tissue freezing medium (Ted Pella, Redding, CA) and frozen in powdered dry ice. The brains were sectioned (at 10-μm thickness) in a Microm cryostat, thaw-mounted onto VWR micro slides, and the sections were stored at −20°C until hybridization. Semiadjacent sections throughout the brain were hybridized with [^{35}S]-labeled cRNA sense and antisense probes for detection and localization of VEGF mRNA according to our previously published protocol (41–43). The VEGF cDNA plasmid [kindly provided by L.F. Brown, Harvard University (44)] was contained in a pGEM3 vector and consisted of 393 bp. Labeled probes were prepared by in vitro transcription from linerized cDNA plasmids using the proper RNA polymerase (T7 for antisense and SP6 for sense) in the presence of excess [^{35}S]-UTP (PerkinElmer, Waltham, MA) and were generated as previously described (41). Slide-mounted sections were hybridized overnight at 60°C in hybridization mixture containing the [^{35}S]-labeled probe at a concentration of 1×10^6 cpm/50 μl/slide. After posthybridization treatment, slides were exposed to BioMax MR film (Kodak, Rochester, NY) for 8 d for generation of film autoradiographs. The films were developed with Kodak GPX developer and fixer. Semiquantitative analysis of the hippocampal dentate gyrus ipsilateral to the hemisphere of TMEV infection was performed using OD measurements (Scion Image software [National Institutes of Health]). The mean corrected gray levels were generated by subtracting a background measurement (taken from a nontissue-containing area on the same slide) from the OD in the dentate gyrus for each section. To provide cellular resolution, slides were then dipped in Kodak NTB autoradiography emulsion, exposed for 20 d, and then developed with Kodak D19 developer. These sections were counterstained with cresyl violet and cover-slipped for further analysis. Additional sections hybridized with the [^{35}S]-labeled control sense probe resulted in no specific cellular labeling.

Immunofluorescent microscopy

Fresh-frozen brains were sectioned (10-μm thickness) in a −20°C Microm cryostat and thaw-mounted onto VWR micro slides. Mounted sections were stored at −20°C. Tissue sections were fixed in cold 95% ethanol at 4°C for 15 min and washed with repeated changes in 0.1 M PBS for 30 min. Sections were blocked in 10% normal goat serum (in 0.1 M PBS + 0.03% Triton X-100) for 1 h. Sections were incubated in mouse antineuronal nuclei (NeuN) (1:1000) (Chemicon Millipore, Billerica, MA) and rat anti-CD8 α (1:1000) (AbD Serotec, Raleigh, NC) or rabbit anti-VEGF (1:200) (Calbiochem) overnight at 4°C in humid chamber. Sections were washed in 0.1 M PBS for 1 h and incubated in Alexa Fluor 647 goat anti-mouse IgG (1:750; Invitrogen, Carlsbad, CA), Alexa Fluor 555 goat anti-rat IgG (1:750; Invitrogen), or Alexa

Flour 647 goat anti-rabbit IgG (1:750; Invitrogen) for 4 h at room temperature. Slides were washed in 0.1 M PBS at 4°C overnight. Slides were incubated in 70%, 95%, and 100% ethanol for 3 min each and xylene for 5 min. Slides were coversliped using Vectashield mounting medium for fluorescence (H-1000; Vector Labs, Burlingame, CA). Sections were imaged at room temperature at ×20 magnification using a Zeiss LSM 510 laser scanning confocal microscope at the Center for Biological Microscopy at the University of Cincinnati, College of Medicine, and Zeiss LSM 510 Image Browser version 4.0.0.241 (Carl Zeiss Micro Imaging, Oberkochen, Germany).

Magnetic resonance imaging

Animal handling and imaging were in compliance with Children's Hospital Research Foundation Institutional Animal Care and Use Committee protocol 7A04035 approved March 8, 2008. Groups of four mice were sedated using 1.5% isofluorane delivered with 0.4 l/min of medical air. Magnetic resonance imaging (MRI) was performed on a Bruker 70/30 USR Biospec microimager/spectrometer (Bruker Biospin, Ettlingen, Germany) using a B-GA12 gradient insert (400 mT/m), 38 mm linear proton volume. For body scans, T1-weighted spin-echo images (TR/TE = 500/10 ms, field of view = 2.56 × 2.56 cm, matrix = 256 × 128) with two averages were used. The resulting spatial resolution is 100 × 200 μm with a 1-mm slice thickness. For brain scans, T1-weighted spin-echo sequences (TR 200 ms, TE 10 ms, field of view: 4 × 2.5 × 2.5 cm, matrix: 256 × 128 × 128, NEX 2) were used to determine the overall volume of gadolinium-enhancing areas (areas of increased BBB permeability). The mice were first imaged without contrast, removed from the scanner, and administered 0.1 mM/kg gadopentate dimeglumine (Magnevist, Berlex Laboratories, Montville, NJ) via tail vein injection, inserted back into the scanner and the imaging protocol was repeated.

Statistical analysis

Mean and SE values for FITC-albumin measurements, Western blot measurements, and in situ hybridization measurements were calculated using software program SigmaStat (SYSTAT Software, Chicago, IL). Bar graphs with SE values were plotted on software program SigmaPlot (SYSTAT Software). To determine significance between groups, a Student *t* test was performed using SigmaPlot with the exception of occludin Western blots corrected for GAPDH in which a rank sum test was performed using SigmaStat.

Results

CD8 T cell-mediated vascular permeability is specific to the CNS in this model

Inthe PIFS model ofBBB disruption, the majorityof brain-infiltrating CD8 T cells are specific for the immunodominant D^b:$VP2_{121–130}$ epitope in C57BL/6 mice (22,23). At 7 d post-TMEV infection, this CD8 T cell expansion is predominantly localized to the CNS and not in peripheral lymphoid compartments (19,23). To determine whether vascular permeability in the PIFS model was also exclusively localized to the CNS, we used 7 Tesla whole body MRI 24 h post-administration of $VP2_{121–130}$ peptide to induce BBB disruption or mock E7 control peptide. Prior to scanning, gadolinium was i.v. injected to enable visualization of vascular leakage in major organs. As previously reported using contrast-enhanced T1-weighted MRI at 24 h post-$VP2_{121–130}$ administration, we observe extensive gadolinium leakage into the brain but not into mock E7 peptide-administered controls (Fig. 1*A*, 1*D* show a representative mouse of four animals scanned) (22,45). However, whole body scans revealed an absence of vascular permeability outside the CNS in both animals administered $VP2_{121–130}$ peptide that were symptomatic for PIFS (Fig. 1*E*, 1*F*) or mockE7 peptide-treated controls (Fig. 1*B*, 1*C*, four animals scanned). Therefore, consistent with our previous histological analysis of pathology in this model (19), this approach demonstrated that vascular permeability induced with PIFS

was not systemic, but rather localized exclusively to the brain, the sight of D^b:$VP2_{121–130}$ epitope-specific CD8 T cell expansion.

Using FITC-albumin leakage as a marker for BBB disruption, we have demonstrated that Ag-specific CD8 T cells initiate BBB disruption (22). To determine the location of CD8 T cells in the CNS during acute TMEV infection, we used immunofluorescent confocal microscopy. Through an analysis of CNS tissue derived from groups of four animals, we determined that $CD8^+$ cells were prevalent throughout the brain during acute TMEV infection. Shown are $CD8^+$ cells infiltrating the hippocampal region (neurons in the stratum granulosum [SG] of the hippocampal dentate gyrus are identified with NeuN staining in blue) in a representative seven day TMEV-infected animal (n = 4 animals, Fig. 2*A*,2*C*, 2*D*). We also demonstrate that 4 h postadministration of $VP2_{121–130}$, there is mild leakage of FITC-albumin (green) from vasculature in the hippocampus where $CD8^+$ cells are found in close proximity to both blood vessels and neuronal cell bodies (n = 4 mice, Fig. 2*B*, 2*E*, 2*F*). This analysis, although not definitive in determining specific molecular interactions, demonstrated that $CD8^+$ cells are colocalizing to both neurons and areas of vascular permeability.

VEGF is expressed prior to peak levels of FITC-albumin leakage into the CNS

VEGF cytokine expression in the CNS is a putative downstream mechanisim by which inflammation could promote CNS vascular permeability (27,38,46). To determine the extent this cytokine was upregulated during CD8 T cell-mediated CNS vascular permeability, we assessed VEGF protein levels and FITC-albumin leakage into the brain at 0, 2, 4, 12, and 24 h post-$VP2_{121–130}$ peptide administration (n = 4 per group). We determined that the 45 kDa form of VEGF protein was significantly increased within 4 h postadministration of $VP2_{121–130}$ peptide when compared with 0 h controls (n = 4 per group; p = 0.004) (Fig. 3*B*). VEGF protein levels remained significantly elevated at 12 (n = 4; $p < 0.01$) and 24 (n = 4; p = 0.01) h postadministration of $VP2_{121–130}$ peptide. CNS vascular permeability in the brain followed similar kinetics as VEGF expression in that a strong trend toward increased leakage of FITC-albumin was observed at 4 h postadministration of $VP2_{121–130}$ peptide (n = 4; p = 0.06). This increase in FITC-albumin leakage became significantly higher than 0 h baseline controls at the 12 h and 24 h time points (n = 4; $p < 0.01$) (Fig. 3*B*). Concomitant with increased VEGF levels and vascular permeability was increased phosphorylation of VEGF receptor flk-1 in brain tissue (Fig. 3*C*). This significant increase in flk-1 phosphorylation occurred at 4 h postadministration of $VP2_{121–130}$ peptide and remained significantly increased at the 12 and 24 h time points (n = 4; $p < 0.01$ when compared with 0 h baseline controls for all groups). The conclusion from these studies was that increased VEGF protein and flk-1 phosphorylation was coinciding with CNS vascular permeability after induction of Ag-specific CD8 T cell-mediated vascular permeability.

Neurons are a major source of VEGF expression in the CNS after induction of CD8 T cell-mediated CNS vascular permeability

To determine the cellular source of VEGF during CNS vascular permeability, we used in situ hybridization to label VEGF mRNA. Gross analysis of coronal brain sections from film autoradiograms revealed that VEGF mRNA expression was increased by 2 h postadministration of $VP2_{121–130}$ when compared with uninfected and 0 h baseline controls (Fig. 4). The intensity of VEGF mRNA labeling remained increased at 4, 12, and 24 h postadministration of $VP2_{121–130}$ peptide (Fig. 4). Because the hippocampus is an area with extensive FITC-albumin leakage and high levels of VEGF protein translation, we semiquantitatively analyzed the SG of the hippocampal dentate gyrus to determine at which time points VEGF mRNA expression was significantly upregulated in this brain region. In Fig. 4*G*, we demonstrate that 2 h post-administration of $VP2_{121–130}$, VEGF mRNA labeling is significantly increased in this area of the brain when compared with the 0 h time point (0, 2 h;

$n = 4$; $p < 0.001$) and continues to be significant at the 4 h ($n = 4$; $p < 0.001$), 12 h ($n = 4$; $p < 0.001$), and 24 h ($n = 4$; $p < 0.001$) time points. We also observed no significant differences in VEGF mRNA expression between un-infected mouse brain, TMEV-infected 0 h control, and sham PBS-injected animals ($n = 4$ per group, Fig. 4*G*), demonstrating that the method of i.c. infection does not elicit VEGF mRNA upregulation in the SG.

Upon further analysis of the hippocampus, we determined that neurons were a major source of VEGF expression during CNS vascular permeability. In Fig. 4*H* and 4*I*, we present VEGF mRNA emulsion autoradiograms of cresyl violet (Nissl)-stained sections. A cell was considered to express VEGF mRNA if there was a concentration of silver grains clustered over the cell body. The vast majority of VEGF cRNA-hybridizing cells within the hippocampal formation displayed Nissl-staining characteristics of neurons (e.g., the small, densely packed granule cells of the dentate gyrus SG; the larger pale-staining nuclei of hilar neurons). Increased expression of VEGF mRNA in the SG did not occur evenly throughout the dentate, but rather was patchy in appearance (Fig. 4*H*). In Fig. 4*I*, we demonstrate morphologically that primarily small granule cells of the hippocampal dentate gyrus, as well as a subpopulation of adjacent hilar neurons, are positive for VEGF mRNA. Patchy expression of VEGF mRNA was also observed within some of the large, pale-staining pyramidal cells of the CA1 and CA3 stratum pyramidale (not shown in Fig. 4*H*, 4*I*). In addition, occasional examples of hybridization over cells with Nissl-staining characteristics of glia (e.g., small, dark nuclei) can be found within the hippocampus, such as within the molecular layers. Thus, it cannot be ruled out that infrequent glia (i.e., astrocytes, microglia) also express VEGF mRNA. We did not, however, observe leukocyte morphologies that expressed VEGF mRNA. However, these in situ hybridization data strongly imply that the major cell type expressing VEGF in the hippocampus is neuronal. Immunofluorescent staining of VEGF protein and the neuronal marker NeuN further confirmed that neurons were a major source of VEGF protein during BBB disruption (Fig. 4*J*, 4*K*, 4*M*). Similar to the in situ mRNA analysis, expression of VEGF protein by neurons was patchy throughout the hippocampal region.

Inhibition of neuropilin-1 with ATWLPRR peptide reduces flk-1 phosphorylation and CNS vascular permeability

To determine whether CNS vascular permeability was mediated through VEGF-related signal transduction, we administered the neuropilin-1 (NRP-1) inhibitor, ATWLPPR. NRP-1 is a coreceptor for the VEGF receptor flk-1. Dimerization of these two receptors has been shown to enhance interaction of VEGF with flk-1, amplifying downstream signal transduction (47–49). In this experiment, we measured levels of FITC-albumin leakage into the brain in 7-d TMEV-infected C57BL/6 mice administered $VP2_{121–130}$ peptide to induce CNS vascular permeability. These animals received either a 1-mg or 3-mg dose regimen of VEGF inhibitor ATWLPPR, sterile PBS, or a 3-mg dose regimen of scrambled (RAPTLWP) peptide mock treatment control. One group was administered mock control E7 peptide i.v. to serve as an additional infected control in which CD8 T cells were not stimulated (22). One hour after FITC-albumin injection, mice were harvested to assess CNS vascular permeability as previously described (Fig. 5*A*) (22). Treatment with PBS, mock peptide RAPTLWP, and 1 mg doses of ATWLPPR resulted in significant increases in FITC-albumin leakage into the brain when compared with negative control E7 peptide-treated animals. However, treatment with 3 mg doses of ATWLPPR significantly decreased leakage of FITC-albumin into the brain when compared with PBS- and RAPTLWP-treated animals ($n = 9$; $p < 0.01$). There was no significant difference between mock E7 peptide-treated and 3 mg ATWLPPR-treated animals (E7 $n = 6$, 3 mg $n = 9$; $p = 0.23$). This experiment demonstrated that administration of NRP-1 inhibitor reduced CD8 T cell-induced CNS vascular permeability.

NRP-1 is a nontyrosine kinase coreceptor for VEGF that has been shown to enhance flk-1-mediated processes (47). Previous reports have shown that peptide inhibitor, ATWLPPR, inhibits binding of VEGF to NRP-1, decreasing flk-1 activation (50,51). To determine, in vivo, whether systemic ATWLPPR administration reduces flk-1 activation in the brain in this model, we used Western blot analysis of flk-1 phosphorylation. Administration of 3 mg doses of ATWLPPR to C57BL/6 mice induced to undergo CNS vascular permeability with administration of $VP2_{121–130}$, peptide significantly reduced phosphorylation of flk-1 when compared with PBS controls ($n = 9$; $p < 0.001$) (Fig. 5*B*). These data implied that decreased flk-1 phosphorylation could be achieved through administration of NRP-1 inhibitor in vivo, coinciding with a reduction in CNS vascular permeability in these animals.

Inhibition of NRP-1 with ATWLPRR peptide preserves BBB tight junction protein occludin

Inhibition of CNS vascular permeability through administration of NRP-1 inhibitor suggested that BBB integrity was preserved. Our group previously reported alteration of the CEC BBB tight junction protein occludin after CD8 T cell-induced CNS vascular permeability (22). In this previous study, we determined that 4 h postadministration of $VP2_{121–130}$ peptide, occludin levels were significantly decreased in the brain coinciding with the onset of vascular permeability (22). We therefore examined occludin levels in microvessel isolations obtained from animals treated with 3 mg doses of ATWLPPR as compared with sterile PBS controls. In accordance with having preserved vascular integrity (Fig. 5*A*), animals treated with ATWLPPR NRP-1 inhibitor had significantly higher levels of occludin in microvessel isolates when compared with sterile PBS-treated animals (PBS $n = 6$, 3 mg $n = 9$) (Fig. 5*C*). These results demonstrate that inhibition of NRP-1 in vivo preserves occludin protein levels in CNS microvessels in the PIFS model.

Perforin is required for VEGF upregulation

Despite having similar CNS infiltration of D^b:$VP2_{121–130}$ Ag-specific CD8 T cells in the brain of wild-type animals, perforin-deficient C57BL/6 mice did not exhibit BBB tight junction protein alterations or CNS vascular permeability in the PIFS model (22). To determine the extent VEGF upregulation is dependent on perforin, 7-d TMEV-infected C57BL/6 perforin$^{-/-}$ mice were administered $VP2_{121–130}$ or mock E7 peptide and assessed for CNS vascular permeability and VEGF expression. In Fig. 6, we demonstrate that there are no differences in VEGF mRNA expression and anatomical location between the E7 peptide (Fig. 6*A*) and $VP2_{121–130}$ peptide treated-animals (Fig. 6*B*). Similarly, we semiquantitatively analyzed VEGF mRNA in the SG of the hippocampal dentate gyrus (Fig. 6*C*) and VEGF protein in the whole brain (Fig. 6*D*) and found no significant differences when compared with the dramatic increases observed in perforin competent wild-type mice in the PIFS model (Fig. 4*F*). These results demonstrate that perforin is necessary for CD8 T cell-mediated upregulation of VEGF in the CNS and the ensuing vascular permeability syndrome (22).

Discussion

VEGF-mediated processes have been implicated in numerous disease states, including cerebral malaria, DHF, traumatic brain injury, meningococcal septic shock, cancer metastases, stroke, and MS (30,32,33,35,52–54). The results of the current studies demonstrate an in vivo role for VEGF in BBB dysregulation and CNS vascular permeability under neuroinflammatory conditions. Using this model, we have also demonstrated that CD8 T cells can initiate upregulation of neuronal expression of VEGF in the CNS through a process requiring perforin expression. To our knowledge, we are the first to demonstrate modulation of VEGF expression in neurons through stimulating CNS-infiltrating CD8 T cells.

Clinical studies of human cerebral malaria have shown that the BBB is altered during infection similar to results observed in our model (6). Animal models of cerebral malaria have put forth the hypothesis that CD8 T cells are involved in neuropathology and CNS vascular permeability (16). Interestingly, studies using tissue from human cerebral malaria patients show a prominent population of VEGF-expressing cells in the CNS when compared with controls, suggesting a role for this protein in the neuropathology associated with this disease (33). Unlike human and mouse cerebral malaria models, the CD8 T cell-specific Ag has been identified in our system. This is advantageous as it enables us to determine the kinetics of inflammatory mediators downstream of stimulation of CNS-infiltrating CD8 T cells to serve as a model for human neurologic diseases that imply a causal role for CD8 T cells. BBB disruption in this model is specifically the result of the CD8 T cell reaction to i.v. administration of TMEV-derived $VP2_{121–130}$ peptide Ag.

Human viral hemorrhagic fevers also present with abnormal CD8 T cell activity. In DHF, Ag-specific CD8 T cell activation and expansion can be measured in the blood of patients during the peak of this fatal hemorrhagic syndrome (10). It has been put forward that VEGF and VEGFR2, the human homolog of flk-1, may play an important role in this condition. Studies of plasma in human dengue patients have shown that vascular permeability is inversely correlated with the amount of soluble VEGFR2. Levels of plasma soluble VEGFR1 were stable, indicating that VEGFR2 is the key receptor involved in DHF (35). When these studies were evaluated using an in vitro system, it was demonstrated that the dengue virus suppressed soluble VEGFR2 levels, while promoting increased levels of membrane-bound VEGFR2 (35). These findings are intriguing and suggest that increased levels of membrane bound VEGFR2 may lead to enhanced signaling of vascular permeability-inducing pathways during dengue infection (35). To determine the extent that VEGF-related pathways potentiated vascular permeability in the PIFS model, we first sought to determine the cellular source and time course of VEGF upregulation. To determine this, we used Western blot and in situ hybridization techniques. Our results indicate that VEGF protein and flk-1 activation are significantly increased in the PIFS model by 4 h post-$VP2_{121–130}$ administration, coinciding with the onset of CNS vascular permeability.

We determined in these studies that neurons rapidly upregulated VEGF after induction of PIFS. We semiquantitatively analyzed VEGF mRNA expression in the SG of the hippocampal dentate gyrus and found that VEGF mRNA was significantly increased by 2 h postadministration of $VP2_{121–130}$ and continued to be significant through 24 h. VEGF expression therefore preceded and coincided with vascular permeability. We therefore i.v. administered a NRP-1 inhibitor, ATWLPPR, which has been shown to prevent flk-1-mediated mechanisms in vitro and in vivo (50,51). NRP-1 is a nontyrosine kinase VEGF receptor that enhances VEGF binding to flk-1 and subsequent flk-1-mediated mechanisms (47,50,55). Our results demonstrate that i.v. administration of high doses of ATWLPPR preserves CNS vascular integrity in this model as assessed by comparing leakage of FITC-albumin into the brain with saline- and scrambled peptide-treated animals. The results of these experiments provide evidence that engagement of VEGF with its receptors, NRP-1 and flk-1 significantly contributes to CD8 T cell-driven CNS vascular permeability.

Tight junction protein expression in microvessels is dynamically altered after induction of PIFS (22). In particular, levels of tight junction protein occludin are rapidly reduced in brain microvessels after induction of CD8 T cell-mediated CNS vascular permeability (22). The importance of occludin and other tight junction proteins in BBB disruption is an emerging area of research. There are currently three models in which occludin is modified during BBB disruption: 1) phosphorylation by ρ kinases (56), 2) altered location in vascular endothelial cells (57), and 3) reduction in total protein levels (22,40,58). These three models are not mutually exclusive of one another, as both phosphorylation and reduction of occludin have

been reported simultaneously in BBB dysregulation (59). Here, we demonstrate that peptide inhibition of the interaction of VEGF with NRP-1 results in preservation of occludin protein when compared with the saline controls at 24 h postinduction of PIFS (Fig. 5). This finding further supports a working model in which preserved occludin protein levels contribute to maintaining an impermeable BBB. These data also support the concept that VEGF-related signal transduction through NRP-1 and flk-1 contributes to alterations in microvessel occludin protein levels in T cell-induced BBB disruption.

Recently, we reported that the immune effector protein, perforin, was necessary for CNS vascular permeability to occur in this model (22). Perforin, a cytolytic protein, is used by CD8 (cytotoxic) T lymphotcytes and NK cells to deliver inflammatory mediators that control virus infection (60). In this study, we demonstrate that VEGF upregulation is dependent on perforin expression. This observation necessitates further analysis of the cellular source of perforin and defining the critical agent delivered through this pathway. Similar to our studies, Kim et al. observed a reduction in CNS vascular permeability in perforin-deficient lymphocytic choriomeningitis virus-infected mice (61). However, the authors concluded that delayed onset of CNS vascular permeability in perforin-deficient mice was due to reduced infiltration of CD8 T cells into the CNS (61,62). The authors instead concluded through GR-1 depletion strategies that neutrophils were the critical blood-derived cell type promoting BBB disruption. However, our studies do not support this hypothesis. In previous studies with this model, we demonstrate similar levels of CNS infiltration of Ag-specific CD8 T cells in the brains of 7-d-old TMEV-infected C57BL/6 and C57BL/6 perforin-deficient mice (22,23). This indicated that delayed recruitment of CD8 T cells to the CNS is not responsible for lack of BBB dysregulation in perforin-deficient animals in the PIFS model. Furthermore, we have determined that the majority of D^b:$VP2_{121–130}$ epitope-specific CD8 T cells express surface GR-1 protein (data not shown). For this reason, it remains possible that GR-1-specific Ab depletion could have removed large numbers of activated CD8 T cells in addition to neutrophils in the BBB studies conducted using lymphocytic choriomeningitis virus (61).

Matrix metalloproteinases (MMPs) are extracellular matrix degrading enzymes that facilitate BBB disruption, trafficking of immune cells into the CNS, as well as vascular remodeling (63). Among this family of proteases, MMP-2, MMP-3 and MMP-9 are linked to basal lamina degradation that result in tight junction protein alterations and vascular permeability (63). These proteases are very pleiotropic in the CNS and are easily up regulated in astrocyte and microglial cultures (63–67). Furthermore, it has been shown recently that hematopoietically expressed MMP-9 can contribute to BBB disruption in a murine model of ischemia (68). Meanwhile, studies using MMP-3 knockout mice presented with reduced BBB disruption after intracerebral injection with LPS (69). These findings support a role for blood derived cells and inflammation in promoting BBB disruption through the expression of MMPs and serve as an additional link between immune cells and CNS vascular permeability in addition to the findings put forward in this study.

In conclusion, we demonstrate that under neuroinflammatory conditions, the inflammatory mediators perforin, VEGF, NRP-1, and flk-1 contribute to BBB disruption. In our analysis, we have also determined that a major cell type that upregulates VEGF expression in this process is neuronal. We have incorporated these factors into a working model by which Ag-specific CD8 T cells initiate BBB disruption. Our direct hypothesis entails a mechanism in which CD8 T cells using perforin directly engage neurons to promote VEGF upregulation. Neuronal processes are an integral part of the neurovascular unit (70). Therefore, neuronally expressed VEGF could be delivered to CECs and alter tight junctions of the BBB. Our indirect hypothesis entails CD8 T cells engaging an alternative cell type in the CNS which then induces VEGF expression. VEGF expression is not exclusive to neurons, leaving the potential for other CNS cell types, endothelial cells, and immune cells to contribute to BBB disruption through

expression of this cytokine (71). Induction of VEGF through either the direct and indirect pathways outlined previously promotes vascular permeability through flk-1/NRP-1 receptor-mediated signal transduction. This, likely, results in MMP protease activity and BBB tight junction alterations and vascular permeability. Assessment of the direct and indirect mechanisms in vivo requires the development of the appropriate conditional knockout mice which are currently under development. Nevertheless, the data put forward provide rationale for the inhibition of VEGF-mediated pathways as a therapeutic strategy designed to treat neurologic conditions associated with immune-mediated CNS vascular permeability.

Acknowledgments

This work was supported by National Institutes of Health Grants NS058698 and NS060881, the University of Cincinnati Neuroscience Institute, and The Waddell Center for Multiple Sclerosis.

We thank Scott Holland and Scott Dunn of Cincinnati Children's Hospital and Medical Center for MRI technical assistance, Nancy Kleene and Birgit Ehmer of the University of Cincinnati for microscopy expertise, Tracy A. Brooks and Thomas P. Davis of the University of Arizona for assistance with the microvessel isolation protocol. Finally, we thank Lawrence F. Brown of Harvard for kindly providing VEGF probes for in situ hybridization.

Abbreviations in this paper

BBB	blood-brain barrier
CEC	cerebral endothelial cell
DHF	dengue hemorrhagic fever
flk-1	fetal liver kinase-1
MMP	matrix metalloproteinase
MRI	magnetic resonance imaging
MS	multiple sclerosis
NeuN	neuronal nuclei
NRP-1	neuropilin-1
PIFS	peptide-induced fatal syndrome
SG	stratum granulosum
TMEV	Theiler's murine encephalomyelitis virus
VEGF	vascular endothelial growth factor
VP	viral peptide

References

1. Medana IM, Turner GD. Human cerebral malaria and the blood-brain barrier. Int J Parasitol 2006;36:555–568. [PubMed: 16616145]
2. Suidan GL, Pirko I, Johnson AJ. A potential role for CD8+ T-cells as regulators of CNS vascular permeability. Neurol Res 2006;28:250–255. [PubMed: 16687049]
3. Huber JD, Egleton RD, Davis TP. Molecular physiology and pathophysiology of tight junctions in the blood-brain barrier. Trends Neurosci 2001;24:719–725. [PubMed: 11718877]
4. Abbott NJ. Astrocyte-endothelial interactions and blood-brain barrier permeability. J Anat 2002;200:629–638. [PubMed: 12162730]
5. Kabakus N, Gurgoze MK, Yildirim H, Godekmerdan A, Aydin M. Acute hemorrhagic leukoencephalitis manifesting as intracerebral hemorrhage associated with herpes simplex virus type I. J Trop Pediatr 2005;51:245–249. [PubMed: 15917264]

6. Brown H, Hien TT, Day N, Mai NT, Chuong LV, Chau TT, Loc PP, Phu NH, Bethell D, Farrar J, et al. Evidence of blood-brain barrier dysfunction in human cerebral malaria. Neuropathol Appl Neurobiol 1999;25:331–340. [PubMed: 10476050]
7. Marchi N, Oby E, Batra A, Uva L, De Curtis M, Hernandez N, Van Boxel-Dezaire A, Najm I, Janigro D. In vivo and in vitro effects of pilocarpine: relevance to ictogenesis. Epilepsia 2007;48:1934–1946. [PubMed: 17645533]
8. Ballabh P, Braun A, Nedergaard M. The blood-brain barrier: an overview: structure, regulation, and clinical implications. Neurobiol Dis 2004;16:1–13. [PubMed: 15207256]
9. Minagar A, Alexander JS. Blood-brain barrier disruption in multiple sclerosis. Mult Scler 2003;9:540–549. [PubMed: 14664465]
10. Mongkolsapaya J, Dejnirattisai W, Xu XN, Vasanawathana S, Tangthawornchaikul N, Chairunsri A, Sawasdivorn S, Duangchinda T, Dong T, Rowland-Jones S, et al. Original antigenic sin and apoptosis in the pathogenesis of dengue hemorrhagic fever. Nat Med 2003;9:921–927. [PubMed: 12808447]
11. Hunt NH, Golenser J, Chan-Ling T, Parekh S, Rae C, Potter S, Medana IM, Miu J, Ball HJ. Immunopathogenesis of cerebral malaria. Int J Parasitol 2006;36:569–582. [PubMed: 16678181]
12. McBride WJ, Bielefeldt-Ohmann H. Dengue viral infections; pathogenesis and epidemiology. Microbes Infect 2000;2:1041–1050. [PubMed: 10967284]
13. Sangkawibha N, Rojanasuphot S, Ahandrik S, Viriyapongse S, Jatanasen S, Salitul V, Phanthumachinda B, Halstead SB. Risk factors in dengue shock syndrome: a prospective epidemiologic study in Rayong, Thailand. I. The 1980 outbreak. Am J Epidemiol 1984;120:653–669. [PubMed: 6496446]
14. Thein S, Aung MM, Shwe TN, Aye M, Zaw A, Aye K, Aye KM, Aaskov J. Risk factors in dengue shock syndrome. Am J Trop Med Hyg 1997;56:566–572. [PubMed: 9180609]
15. Loke H, Bethell DB, Phuong CX, Dung M, Schneider J, White NJ, Day NP, Farrar J, Hill AV. Strong HLA class I—restricted T cell responses in dengue hemorrhagic fever: a double-edged sword? J Infect Dis 2001;184:1369–1373. [PubMed: 11709777]
16. Potter S, Chan-Ling T, Ball HJ, Mansour H, Mitchell A, Maluish L, Hunt NH. Perforin mediated apoptosis of cerebral microvascular endothelial cells during experimental cerebral malaria. Int J Parasitol 2006;36:485–496. [PubMed: 16500656]
17. Nitcheu J, Bonduelle O, Combadiere C, Tefit M, Seilhean D, Mazier D, Combadiere B. Perforin-dependent brain-infiltrating cytotoxic CD8+ T lymphocytes mediate experimental cerebral malaria pathogenesis. J Immunol 2003;170:2221–2228. [PubMed: 12574396]
18. Gillrie MR, Krishnegowda G, Lee K, Buret AG, Robbins SM, Looareesuwan S, Gowda DC, Ho M. Src-family kinase dependent disruption of endothelial barrier function by *Plasmodium falciparum* merozoite proteins. Blood 2007;110:3426–3435. [PubMed: 17693580]
19. Johnson AJ, Mendez-Fernandez Y, Moyer AM, Sloma CR, Pirko I, Block MS, Rodriguez M, Pease LR. Antigen-specific CD8+ T cells mediate a peptide-induced fatal syndrome. J Immunol 2005;174:6854–6862. [PubMed: 15905527]
20. Rodriguez M, Oleszak E, Leibowitz J. Theiler's murine encephalomyelitis: a model of demyelination and persistence of virus. Crit Rev Immunol 1987;7:325–365. [PubMed: 2827957]
21. McDole J, Johnson AJ, Pirko I. The role of CD8+ T-cells in lesion formation and axonal dysfunction in multiple sclerosis. Neurol Res 2006;28:256–261. [PubMed: 16687050]
22. Suidan GL, McDole JR, Chen Y, Pirko I, Johnson AJ. Induction of blood brain barrier tight junction protein alterations by CD8 T cells. PLoS One 2008;3:e3037. [PubMed: 18725947]
23. Johnson AJ, Njenga MK, Hansen MJ, Kuhns ST, Chen L, Rodriguez M, Pease LR. Prevalent class I-restricted T-cell response to the Theiler's virus epitope Db:VP2121-130 in the absence of endogenous CD4 help, tumor necrosis factor α, γ interferon, perforin, or costimulation through CD28. J Virol 1999;73:3702–3708. [PubMed: 10196262]
24. Johnson AJ, Upshaw J, Pavelko KD, Rodriguez M, Pease LR. Preservation of motor function by inhibition of CD8+ virus peptide-specific T cells in Theiler's virus infection. FASEB J 2001;15:2760–2762. [PubMed: 11606479]
25. Senger DR, Galli SJ, Dvorak AM, Perruzzi CA, Harvey VS, Dvorak HF. Tumor cells secrete a vascular permeability factor that promotes accumulation of ascites fluid. Science 1983;219:983–985. [PubMed: 6823562]

26. Krum JM, Khaibullina A. Inhibition of endogenous VEGF impedes revascularization and astroglial proliferation: roles for VEGF in brain repair. Exp Neurol 2003;181:241–257. [PubMed: 12781997]
27. Proescholdt MA, Heiss JD, Walbridge S, Mühlhauser J, Capogrossi MC, Oldfield EH, Merrill MJ. Vascular endothelial growth factor (VEGF) modulates vascular permeability and inflammation in rat brain. J Neuropathol Exp Neurol 1999;58:613–627. [PubMed: 10374752]
28. Ferrara N, Gerber HP, LeCouter J. The biology of VEGF and its receptors. Nat Med 2003;9:669–676. [PubMed: 12778165]
29. Proescholdt MA, Jacobson S, Tresser N, Oldfield EH, Merrill MJ. Vascular endothelial growth factor is expressed in multiple sclerosis plaques and can induce inflammatory lesions in experimental allergic encephalomyelitis rats. J Neuropathol Exp Neurol 2002;61:914–925. [PubMed: 12387457]
30. Su JJ, Osoegawa M, Matsuoka T, Minohara M, Tanaka M, Ishizu T, Mihara F, Taniwaki T, Kira J. Upregulation of vascular growth factors in multiple sclerosis: correlation with MRI findings. J Neurol Sci 2006;243:21–30. [PubMed: 16376944]
31. Krum JM, Mani N, Rosenstein JM. Roles of the endogenous VEGF receptors flt-1 and flk-1 in astroglial and vascular remodeling after brain injury. Exp Neurol 2008;212:108–117. [PubMed: 18482723]
32. Lafuente JV, Argandoña EG, Mitre B. VEGFR-2 expression in brain injury: its distribution related to brain-blood barrier markers. J Neural Transm 2006;113:487–496. [PubMed: 16550327]
33. Deininger MH, Winkler S, Kremsner PG, Meyermann R, Schluesener HJ. Angiogenic proteins in brains of patients who died with cerebral malaria. J Neuroimmunol 2003;142:101–111. [PubMed: 14512169]
34. Zhang ZG, Zhang L, Jiang Q, Zhang R, Davies K, Powers C, Bruggen N, Chopp M. VEGF enhances angiogenesis and promotes blood-brain barrier leakage in the ischemic brain. J Clin Invest 2000;106:829–838. [PubMed: 11018070]
35. Srikiatkhachorn A, Ajariyakhajorn C, Endy TP, Kalayanarooj S, Libraty DH, Green S, Ennis FA, Rothman AL. Virus-induced decline in soluble vascular endothelial growth receptor 2 is associated with plasma leakage in dengue hemorrhagic fever. J Virol 2007;81:1592–1600. [PubMed: 17151115]
36. Chi OZ, Hunter C, Liu X, Weiss HR. Effects of VEGF and nitric oxide synthase inhibition on blood-brain barrier disruption in the ischemic and non-ischemic cerebral cortex. Neurol Res 2005;27:864–868. [PubMed: 16354548]
37. Antonetti DA, Barber AJ, Khin S, Lieth E, Tarbell JM, Gardner TW. Penn State Retina Research Group. Vascular permeability in experimental diabetes is associated with reduced endothelial occludin content: vascular endothelial growth factor decreases occludin in retinal endothelial cells. Diabetes 1998;47:1953–1959. [PubMed: 9836530]
38. Antonetti DA, Barber AJ, Hollinger LA, Wolpert EB, Gardner TW. Vascular endothelial growth factor induces rapid phosphorylation of tight junction proteins occludin and zonula occluden 1. A potential mechanism for vascular permeability in diabetic retinopathy and tumors. J Biol Chem 1999;274:23463–23467. [PubMed: 10438525]
39. Cleveland DW, Fischer SG, Kirschner MW, Laemmli UK. Peptide mapping by limited proteolysis in sodium dodecyl sulfate and analysis by gel electrophoresis. J Biol Chem 1977;252:1102–1106. [PubMed: 320200]
40. Brooks TA, Hawkins BT, Huber JD, Egleton RD, Davis TP. Chronic inflammatory pain leads to increased blood-brain barrier permeability and tight junction protein alterations. Am J Physiol Heart Circ Physiol 2005;289:H738–H743. [PubMed: 15792985]
41. Seroogy, KB.; Herman, JP. In situ hybridization approaches to the study of the nervous system. In: Turner, AJ.; Bachelard, HS., editors. Neurochemistry: A Practical Approach. 2. Oxford University Press; Oxford: 1997. p. 121-150.
42. Numan S, Gall CM, Seroogy KB. Developmental expression of neurotrophins and their receptors in postnatal rat ventral midbrain. J Mol Neurosci 2005;27:245–260. [PubMed: 16186635]
43. Numan S, Seroogy KB. Expression of trkB and trkC mRNAs by adult midbrain dopamine neurons: a double-label in situ hybridization study. J Comp Neurol 1999;403:295–308. [PubMed: 9886032]
44. Detmar M, Velasco P, Richard L, Claffey KP, Streit M, Riccardi L, Skobe M, Brown LF. Expression of vascular endothelial growth factor induces an invasive phenotype in human squamous cell carcinomas. Am J Pathol 2000;156:159–167. [PubMed: 10623663]

45. Pirko I, Suidan GL, Rodriguez M, Johnson AJ. Acute hemorrhagic demyelination in a murine model of multiple sclerosis. J Neuroinflammation 2008;5:31. [PubMed: 18606015]
46. van Bruggen N, Thibodeaux H, Palmer JT, Lee WP, Fu L, Cairns B, Tumas D, Gerlai R, Williams SP, van Lookeren Campagne M, et al. VEGF antagonism reduces edema formation and tissue damage after ischemia/reperfusion injury in the mouse brain. J Clin Invest 1999;104:1613–1620. [PubMed: 10587525]
47. Soker S, Takashima S, Miao HQ, Neufeld G, Klagsbrun M. Neuropilin-1 is expressed by endothelial and tumor cells as an isoform-specific receptor for vascular endothelial growth factor. Cell 1998;92:735–745. [PubMed: 9529250]
48. Wang L, Zeng H, Wang P, Soker S, Mukhopadhyay D. Neuropilin-1-mediated vascular permeability factor/vascular endothelial growth factor-dependent endothelial cell migration. J Biol Chem 2003;278:48848–48860. [PubMed: 14514674]
49. Soker S, Miao HQ, Nomi M, Takashima S, Klagsbrun M. VEGF165 mediates formation of complexes containing VEGFR-2 and neuropilin-1 that enhance VEGF165-receptor binding. J Cell Biochem 2002;85:357–368. [PubMed: 11948691]
50. Starzec A, Vassy R, Martin A, Lecouvey M, Di Benedetto M, Crépin M, Perret GY. Antiangiogenic and antitumor activities of peptide inhibiting the vascular endothelial growth factor binding to neuropilin-1. Life Sci 2006;79:2370–2381. [PubMed: 16959272]
51. Binétruy-Tournaire R, Demangel C, Malavaud B, Vassy R, Rouyre S, Kraemer M, Plouët J, Derbin C, Perret G, Mazié JC. Identification of a peptide blocking vascular endothelial growth factor (VEGF)-mediated angiogenesis. EMBO J 2000;19:1525–1533. [PubMed: 10747021]
52. Sköld MK, von Gertten C, Sandberg-Nordqvist AC, Mathiesen T, Holmin S. VEGF and VEGF receptor expression after experimental brain contusion in rat. J Neurotrauma 2005;22:353–367. [PubMed: 15785231]
53. Pickkers P, Sprong T, Eijk L, Hoeven H, Smits P, Deuren M. Vascular endothelial growth factor is increased during the first 48 hours of human septic shock and correlates with vascular permeability. Shock 2005;24:508–512. [PubMed: 16317379]
54. Weis SM, Cheresh DA. Pathophysiological consequences of VEGF-induced vascular permeability. Nature 2005;437:497–504. [PubMed: 16177780]
55. Gerhardt H, Ruhrberg C, Abramsson A, Fujisawa H, Shima D, Betsholtz C. Neuropilin-1 is required for endothelial tip cell guidance in the developing central nervous system. Dev Dyn 2004;231:503–509. [PubMed: 15376331]
56. Yamamoto M, Ramirez SH, Sato S, Kiyota T, Cerny RL, Kaibuchi K, Persidsky Y, Ikezu T. Phosphorylation of claudin-5 and occludin by ρ kinase in brain endothelial cells. Am J Pathol 2008;172:521–533. [PubMed: 18187566]
57. Dobrogowska DH, Vorbrodt AW. Immunogold localization of tight junctional proteins in normal and osmotically-affected rat blood-brain barrier. J Mol Histol 2004;35:529–539. [PubMed: 15571330]
58. Ronaldson PT, Demarco KM, Sanchez-Covarrubias L, Solinsky CM, Davis TP. Transforming growth factor-β signaling alters substrate permeability and tight junction protein expression at the blood-brain barrier during inflammatory pain. J Cereb Blood Flow Metab 2009;29:1084–1098. [PubMed: 19319146]
59. András IE, Deli MA, Veszelka S, Hayashi K, Hennig B, Toborek M. The NMDA and AMPA/KA receptors are involved in glutamate-induced alterations of occludin expression and phosphorylation in brain endothelial cells. J Cereb Blood Flow Metab 2007;27:1431–1443. [PubMed: 17245419]
60. Voskoboinik I, Trapani JA. Addressing the mysteries of perforin function. Immunol Cell Biol 2006;84:66–71. [PubMed: 16405653]
61. Kim JV, Kang SS, Dustin ML, McGavern DB. Myelomonocytic cell recruitment causes fatal CNS vascular injury during acute viral meningitis. Nature 2009;457:191–195. [PubMed: 19011611]
62. Storm P, Bartholdy C, Sørensen MR, Christensen JP, Thomsen AR. Perforin-deficient CD8+ T cells mediate fatal lymphocytic choriomeningitis despite impaired cytokine production. J Virol 2006;80:1222–1230. [PubMed: 16414999]
63. Candelario-Jalil E, Yang Y, Rosenberg GA. Diverse roles of matrix metalloproteinases and tissue inhibitors of metalloproteinases in neuroinflammation and cerebral ischemia. Neuroscience 2009;158:983–994. [PubMed: 18621108]

64. Gottschall PE, Deb S. Regulation of matrix metalloproteinase expressions in astrocytes, microglia and neurons. Neuroimmunomodulation 1996;3:69–75. [PubMed: 8945720]

65. Rosenberg GA, Cunningham LA, Wallace J, Alexander S, Estrada EY, Grossetete M, Razhagi A, Miller K, Gearing A. Immunohisto-chemistry of matrix metalloproteinases in reperfusion injury to rat brain: activation of MMP-9 linked to stromelysin-1 and microglia in cell cultures. Brain Res 2001;893:104–112. [PubMed: 11222998]

66. Lee WJ, Shin CY, Yoo BK, Ryu JR, Choi EY, Cheong JH, Ryu JH, Ko KH. Induction of matrix metalloproteinase-9 (MMP-9) in lipopolysaccharide-stimulated primary astrocytes is mediated by extracellular signal-regulated protein kinase 1/2 (Erk1/2). Glia 2003;41:15–24. [PubMed: 12465042]

67. Kim KS, Kim HY, Joe EH, Jou I. Matrix metalloproteinase-3 induction in rat brain astrocytes: focus on the role of two AP-1 elements. Biochem J 2008;410:605–611. [PubMed: 18072934]

68. Wang G, Guo Q, Hossain M, Fazio V, Zeynalov E, Janigro D, Mayberg MR, Namura S. Bone marrow-derived cells are the major source of MMP-9 contributing to blood-brain barrier dysfunction and infarct formation after ischemic stroke in mice. Brain Res 2009;1294:183–192. [PubMed: 19646426]

69. Gurney KJ, Estrada EY, Rosenberg GA. Blood-brain barrier disruption by stromelysin-1 facilitates neutrophil infiltration in neuroinflammation. Neurobiol Dis 2006;23:87–96. [PubMed: 16624562]

70. Zlokovic BV. The blood-brain barrier in health and chronic neurodegenerative disorders. Neuron 2008;57:178–201. [PubMed: 18215617]

71. Hermann DM, Zechariah A. Implications of vascular endothelial growth factor for postischemic neurovascular remodeling. J Cereb Blood Flow Metab 2009;29:1620–1643. [PubMed: 19654590]

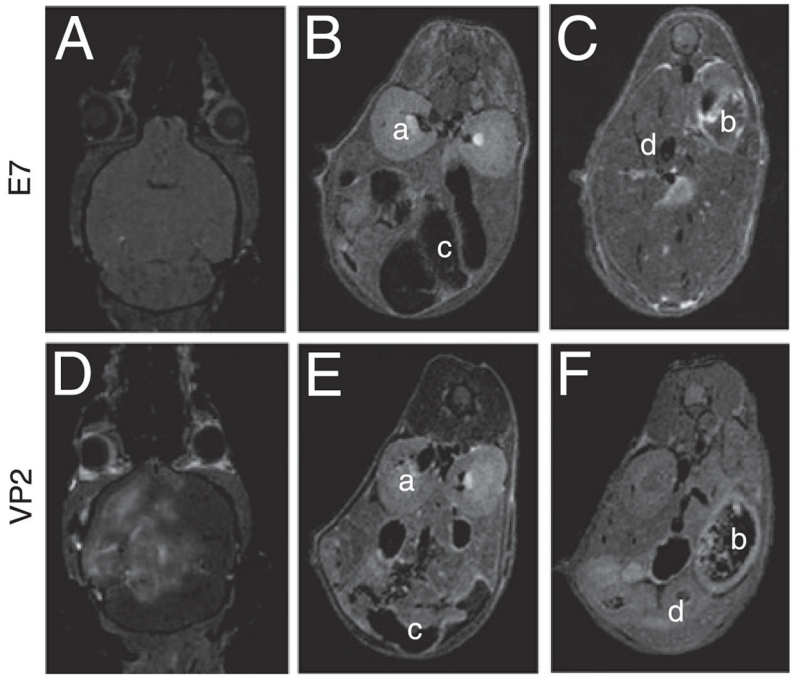

FIGURE 1.

CD8 T cell-mediated vascular permeability is specific to the CNS. At 24 h postadministration of $VP2_{121–130}$ or mock E7 peptide, vascular integrity was assessed in the whole animal using gadolinium-enhanced T1-weighted MRI. At 24 h, there is gadolinium leakage into the brain of (*D*) $VP2_{121–130}$ peptide-administered but not (*A*) E7 peptide-administered animals. Body scans demonstrate a lack of i.v.-injected gadolinium leakage into the peripheral organs with either (*B* and *C*) E7 peptide or (*E* and *F*) $VP2_{121–130}$ peptide-administration ($n = 4$ per treatment group). Examples of major organs include (*a*) kidney, (*b*) spleen, (*c*) intestine, and (*d*) liver. All are negative for gadolinium leakage.

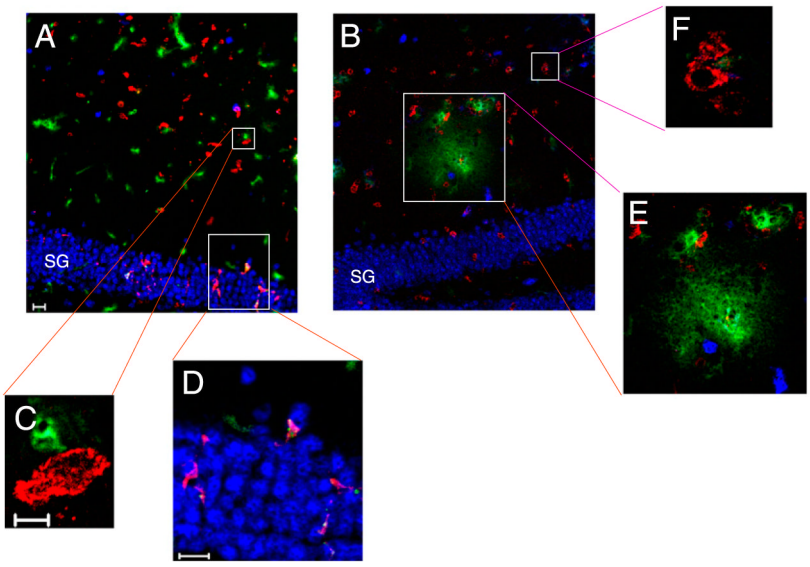

FIGURE 2.

Brain-infiltrating $CD8^+$ cells are in close proximity to neurons and blood vessels during early CNS vascular permeability. Mouse brains isolated from 7-d TMEV-infected mice were immunostained for NeuN (blue) and CD8a protein (red). FITC-albumin (green) was administered i.v. 1 h prior to brain harvest and denotes vessels as well as vascular leakage. *A*, At 0 h, $CD8^+$ cells are detected in the hippocampus (original magnification ×20) in close proximity to (*C*) vessels (original magnification ×100), and (*D*) neurons of the SG of the hippocampal dentate gyrus (original magnification ×40). *B*, FITC-albumin leakage is dorsal to the SG 4 h postadministration of $VP2_{121–130}$ (original magnification ×20). In this region, $CD8^+$ cells are found near (*F*) intact vessels (original magnification ×100) and (*E*) areas with FITC-albumin leakage (original magnification ×40). Shown is a section from a representative mouse of four mice analyzed in each group. Scale bars are as follows: in *A*, 20 μm for *A* and *B*; in *C*, 5 μm for *C* and *F*; in *D*, 20 μm for *D* and *E*.

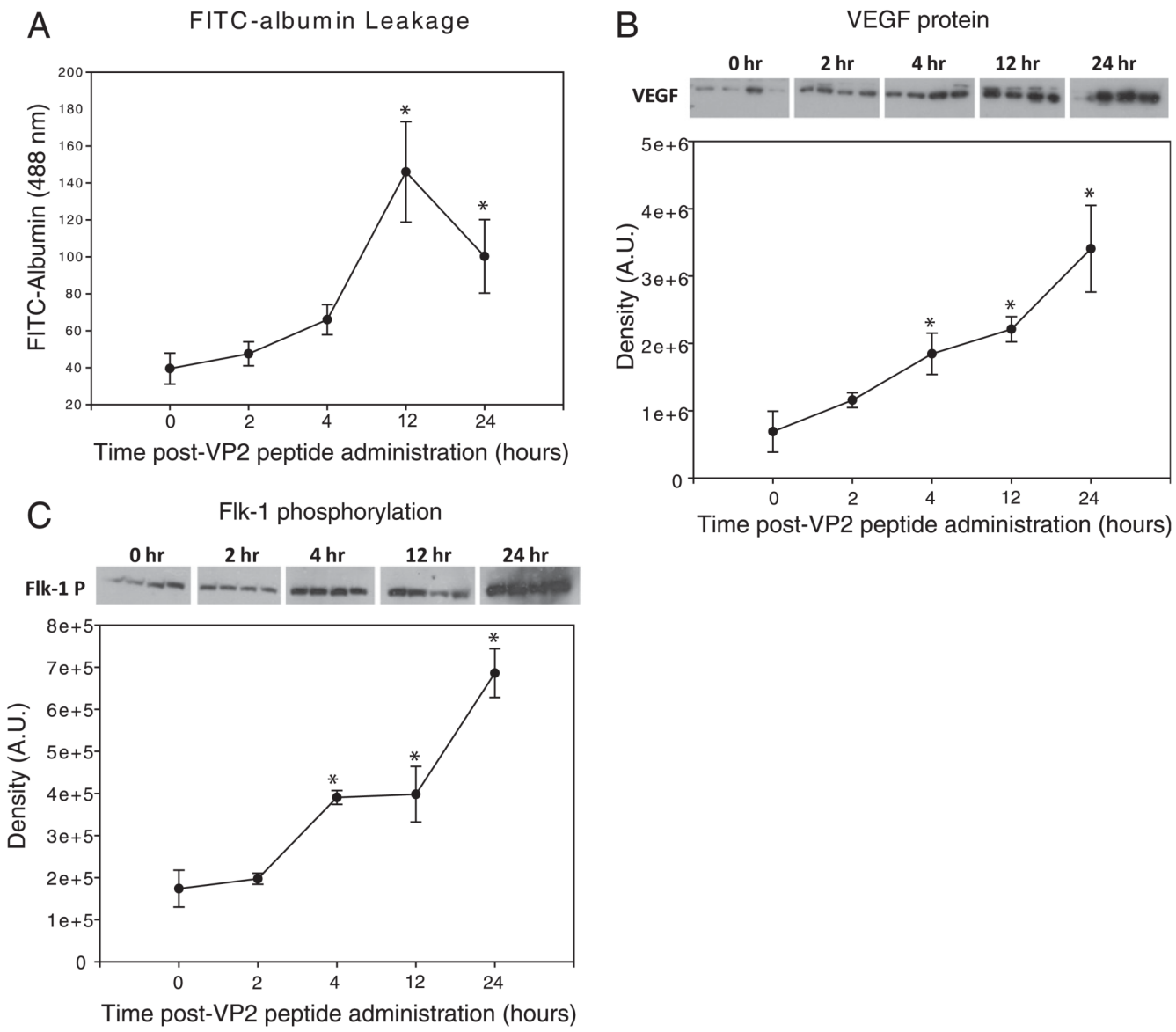

FIGURE 3.

Increased brain VEGF protein and phosphorylation of VEGF receptor flk-1 occur prior to peak levels of CD8 T cell-mediated CNS vascular permeability. At 0, 2, 4, 12, and 24 h postadministration of $VP2_{121–130}$ peptide, C57BL/6 mouse brains were assessed for (*A*) i.v.-injected FITC-albumin leakage into the CNS, (*B*) CNS VEGF protein levels, and (*C*) VEGF receptor, flk-1, phosphorylation. Four animals were assessed at each time point. *Denotes statistical significance with $p < 0.05$ when compared with 0 h baseline controls.

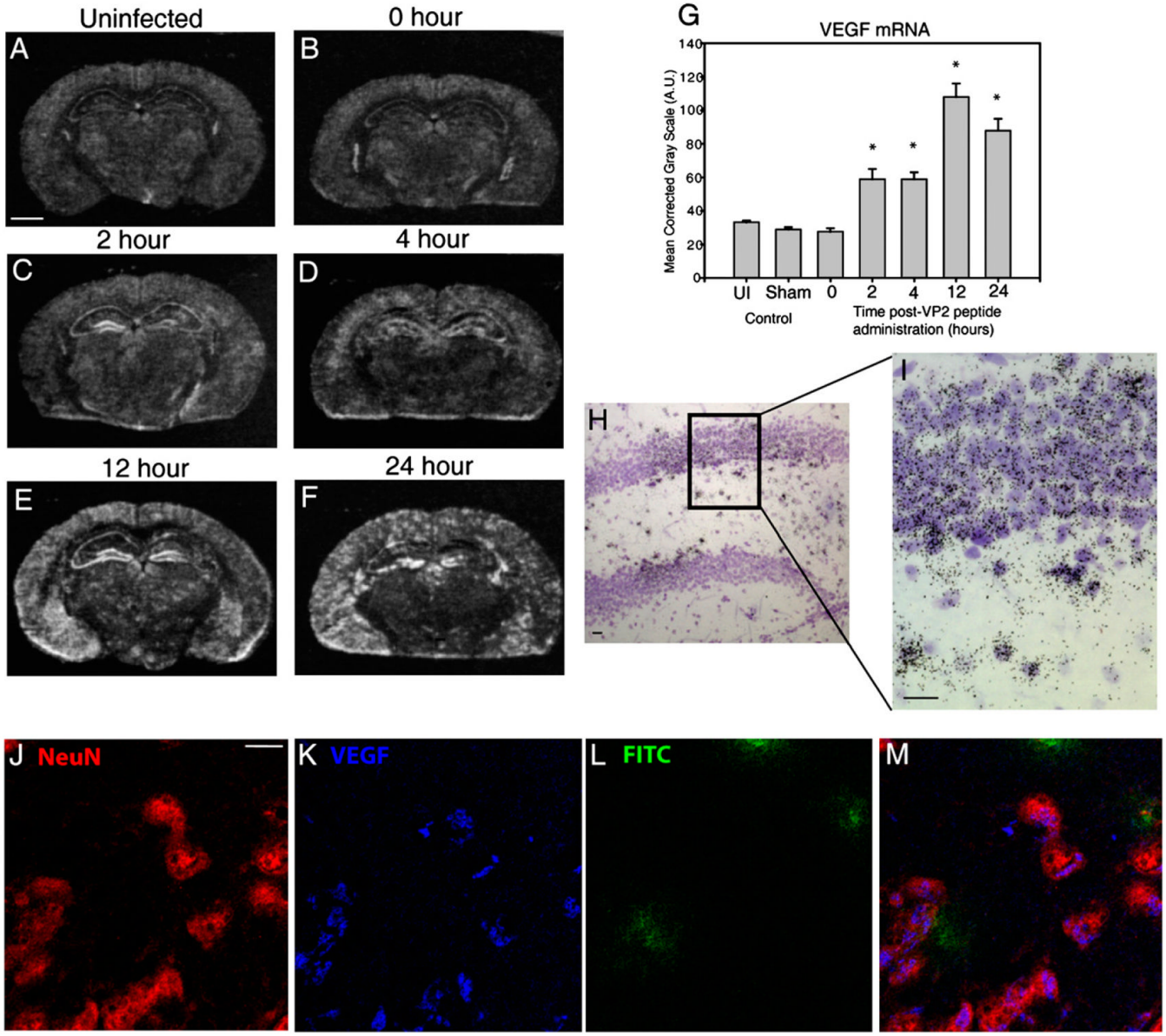

FIGURE 4.

Neurons are a major source of VEGF expression in the CNS after induction of CD8 T cell-mediated CNS vascular permeability. Shown are representative coronal sections of mice at 0, 2, 4, 12, and 24 h postadministration of $VP2_{121–130}$ peptide ($n = 4$ animals per time point). All sections were analyzed for VEGF mRNA and protein expression. In situ hybridization reveals areas of the brain that express VEGF mRNA in (*A*) uninfected, (*B*) 0 h, (*C*) 2 h, (*D*) 4 h, (*E*) 12 h, and (*F*) 24 h post-$VP2_{121–130}$ peptide administration. *G*, VEGF mRNA labeling was quantified in the ipsilateral SG of the hippocampal dentate gyrus. *H* and *I*, Emulsion autoradiographs with cresyl violet counterstaining of the hippocampal dentate gyrus demonstrate substantial VEGF mRNA patchy neuronal labeling in the SG and subjacent hilar region (*H*, original magnification ×20; *I*, original magnification ×40). Also shown is confocal microscopy of (*J*) NeuN, (*K*) VEGF, (*L*) FITC-albumin in hippocampus 12 h postadministration of $VP2_{121–130}$ peptide (original magnification ×100). NeuN immunostaining colocalizes VEGF cytokine as shown merged in (*M*). Scale bars are as follows:

(*A*) 1300 μm for *A–F*, (*H*) 20 μm, (*I*) 20 μm, and (*J*) 10 μm for *J–M*. *Denotes statistical significance with $p < 0.05$ when compared with 0 h.

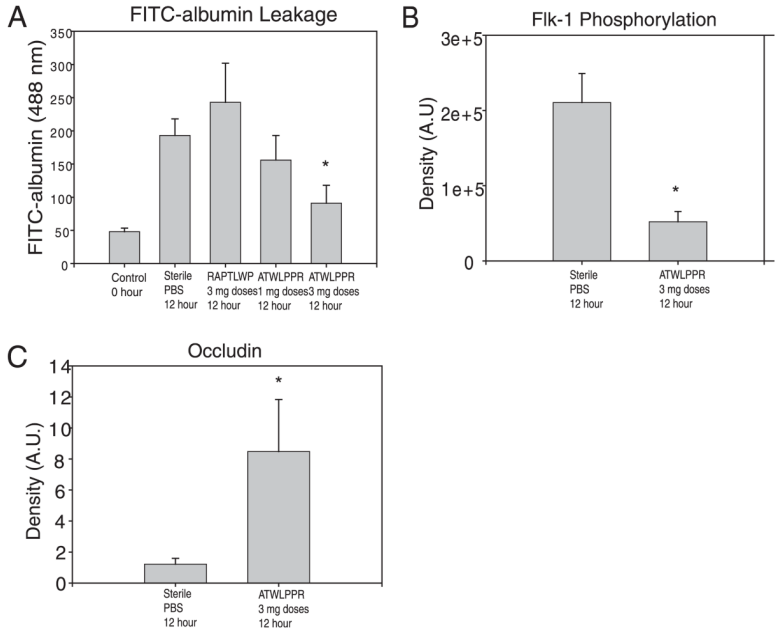

FIGURE 5.

Inhibition of VEGF coreceptor, NRP-1, reduces flk-1 phosphorylation and preserves BBB integrity. At 12 h postadministration of $VP2_{121–130}$ to initiate CNS vascular permeability, C57BL/6 mouse brains were assessed for i.v.-administered FITC-albumin leakage. Mice were treated to 1- or 3-mg dose regimens of NRP-1 inhibitor ATWLPPR, 3 mg doses of mock scrambled peptide RAPTLWP, or sterile PBS (n = 6 animals per treatment group). TMEV-infected mock control E7 peptide-injected animals served as an additional negative control. *A*, Treatment with 3 mg doses of ATWLPPR resulted in significantly less FITC-albumin leakage into the CNS when compared to treatment with RAPTLWP or PBS-administered controls. Treatment with 3 mg doses of ATWLPPR (n = 9 mice) resulted in a significant decrease in (*B*) phosphorylation of flk-1 and preservation of (*C*) CEC BBB tight junction protein occludin levels when compared with PBS-treated animals (n = 6 mice). *Denotes statistical significance with $p < 0.05$ when compared with sterile PBS group.

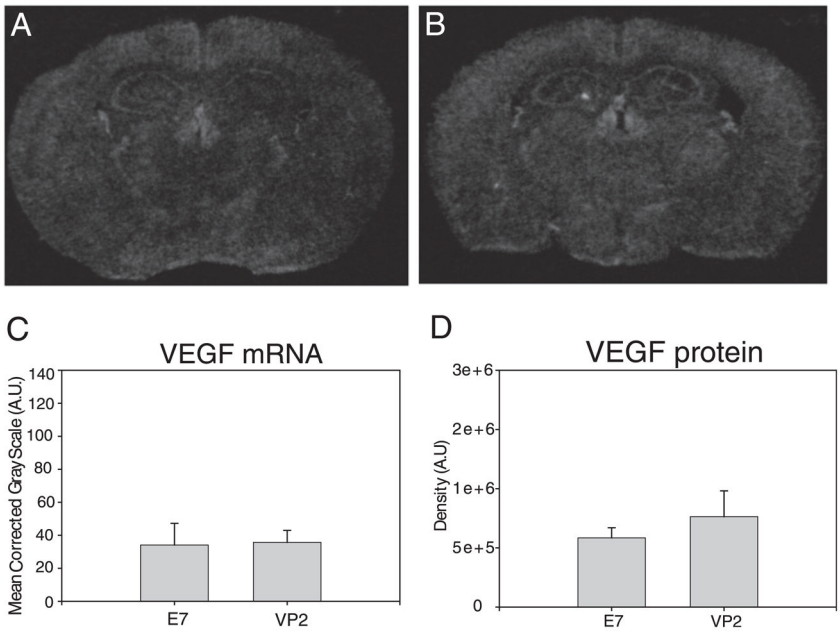

FIGURE 6.

Perforin is required for upregulation of VEGF expression during CD8 T cell-mediated CNS vascular permeability. At 24 h post-administration of (*A*) mock E7 control peptide or (*B*) $VP2_{121–130}$ peptide, C57BL/6 perforin-deficient mouse brains were analyzed for VEGF mRNA using in situ hybridization and VEGF protein using Western blot analysis ($n = 4$ animals for each analysis). *C*, VEGF mRNA in the SG of the hippocampal dentate gyrus and (*D*) VEGF protein levels in the whole brain reveal no changes in VEGF expression in perforin-deficient mice consistent with this strain being resistant to CNS vascular permeability.